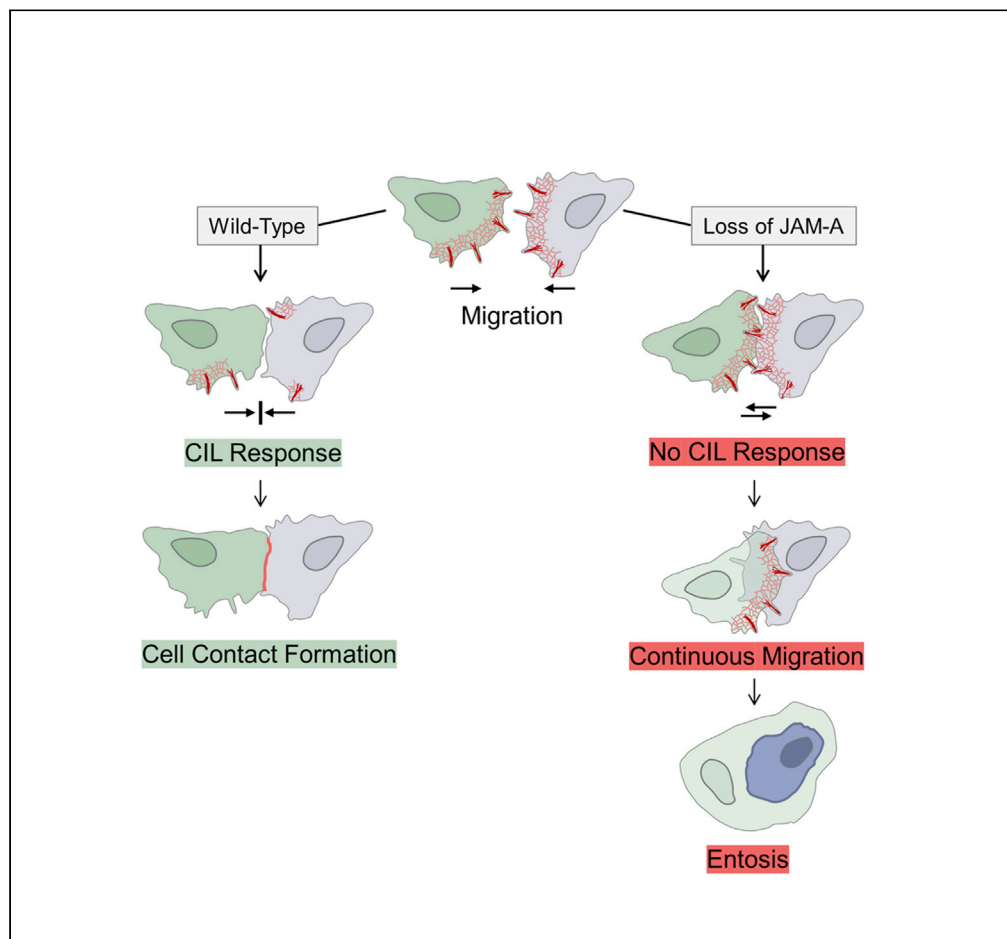**Article**

# Loss of contact inhibition of locomotion in the absence of JAM-A promotes entotic cell engulfment

Mariel F. Schwietzer, Sonja Thölmann, Daniel Kummer, ..., M. Alexander Schmidt, Volker Gerke, Klaus Ebnet

ebnetk@uni-muenster.de

## Highlights

Cell adhesion receptor JAM-A acts as a suppressor of entosis in tumor cells

JAM-A suppresses entosis by recruiting Csk, thus limiting Src activity

Limiting Src activity is required to regulate contact inhibition of locomotion (CIL)

JAM-A links the regulation of CIL to entosis

# iScience

**Article**

# Loss of contact inhibition of locomotion in the absence of JAM-A promotes entotic cell engulfment

Mariel F. Schwietzer,[1,6] Sonja Thölmann,[1,6] Daniel Kummer,[1] Anne Kaschler,[1] Lilo Greune,[2] Eva-Maria Thüring,[1] M. Alexander Schmidt,[2] Volker Gerke,[3] and Klaus Ebnet[1,4,5,7,*]

## SUMMARY

**Entosis is a cell competition process during which tumor cells engulf other tumor cells. It is initiated by metabolic stress or by loss of matrix adhesion, and it provides the winning cell with resources derived from the internalized cell. Using micropatterns as substrates for single cell migration, we find that the depletion of the cell adhesion receptor JAM-A strongly increases the rate of entosis in matrix-adherent cells. The activity of JAM-A in suppressing entosis depends on phosphorylation at Tyr280, which is a binding site for C-terminal Src kinase, and which we have previously found to regulate tumor cell motility and contact inhibition of locomotion (CIL). Loss of JAM-A triggers entosis in matrix-adherent cells but not matrix-deprived cells. Our findings strongly suggest that the increased motility and the perturbed CIL response after the depletion of JAM-A promote entotic cell engulfment, and they link a dysregulation of CIL to entosis in breast cancer cells.**

## INTRODUCTION

Cancer cells have developed a plethora of mechanisms that allow cells to resist the tumor-suppressive activities of the host organism and to survive under conditions of limited nutrient and oxygen supply. For example, anoikis, a cell death program activated in response to the loss of cell-matrix adhesion to prevent cancer cell dissemination (Frisch and Francis, 1994), is antagonized by multiple signaling pathways upregulated in cancer cells (Buchheit et al., 2014). Also, cancer cells undergo profound metabolic reprogramming enabling the cells to scavenge nutrients from nutrient-poor environments (Finicle et al., 2018), and have developed various mechanisms to outcompete other cancer cells as well as non-cancerous cells in the microenvironment (Merino et al., 2016).

Among the various mechanisms involved in cancer cell competition, engulfment of other cells, which results in cell-in-cell structures ("cellular cannibalism") has been proposed to confer metabolic advantages to the "winner" cells (Fais and Overholtzer, 2018). Cell-in-cell structures can occur through an active uptake of a different living cell by a tumor cell through a process that resembles phagocytosis and that has been named phagoptosis (Brown and Neher, 2012; Lugini et al., 2003). Alternatively, cell-in-cell structures can result from an invasion process during which one tumor cell invades another tumor cell of the same type, a process called entosis (Overholtzer et al., 2007). In both cases, the inner cells are, eventually, degraded within a phagolysosomal compartment (Florey et al., 2011; Lugini et al., 2003), leaving the outer cell as the winner cell which benefits from the energy resources provided by the inner cell. Importantly, cell-in-cell structures have been observed in numerous cancers (Fais and Overholtzer, 2018), and the presence of cell-in-cell structures has been associated with advanced cancer stages (Krajcovic et al., 2011; Lugini et al., 2003; Mackay et al., 2018), strongly suggesting that the ability to engulf other cells contributes to the malignant phenotype.

Entosis is characterized by the internalization of a living cell. Internalization is driven by Rho kinase (ROCK)-dependent actomyosin contractility at the rear end of the invading cell, which is required to generate the mechanical tension necessary for invasion (Overholtzer et al., 2007). The internalized cell persists in an entotic vacuole in which it can divide and from which it can escape (Fais and Overholtzer, 2018). The default pathway, however, involves the maturation of the entotic vacuolar membrane through lipidation, followed

[1]Institute-associated Research Group "Cell Adhesion and Cell Polarity", Institute of Medical Biochemistry, ZMBE, University of Münster, Von-Esmarch-Str. 56, 48149 Münster, Germany

[2]Institute of Infectiology, ZMBE, University of Münster, 48149 Münster, Germany

[3]Institute of Medical Biochemistry, ZMBE, University of Münster, 48149 Münster, Germany

[4]Interdisciplinary Clinical Research Center (IZKF), University of Münster, 48149 Münster, Germany

[5]Cells-in-Motion Cluster of Excellence (EXC 1003 - CiM), University of Münster, 48419 Münster, Germany

[6]These authors contributed equally

[7]Lead contact

*Correspondence:
ebnetk@uni-muenster.de

https://doi.org/10.1016/j.isci.2022.105144

by lysosome fusion, death of the cell, and its degradation (Florey et al., 2011). Although apoptosis of the internalized cell has also been observed, specifically when lysosome function or autophagy proteins required for vacuole lipidation are absent (Florey et al., 2011), entotic events observed in clinical cancer specimens were found to occur in the absence of caspase 3 activity defining entosis as non-apoptotic cell death (Overholtzer et al., 2007).

Entosis has been observed in a number of tumor isolates including melanoma and carcinomas of cervix, colon, stomach, and liver (Bozkurt et al., 2021; Overholtzer et al., 2007). On the other hand, entosis is rarely observed in cells grown under regular tissue culture conditions unless cells are detached from the matrix (Durgan and Florey, 2018; Overholtzer et al., 2007), or cells are deprived of nutrients (Hamann et al., 2017). This is most likely owing to the optimized culture conditions under which cells are normally maintained. For example, in two matrix adherent tumor cell lines which readily undergo entosis when cultured in suspension or under conditions of glucose starvation (Hamann et al., 2017; Overholtzer et al., 2007; Sun et al., 2014a; Wang et al., 2016), the rates of entosis are below 2% when grown under regular culture conditions (Garanina et al., 2017). As tumor cells migrating in tissue are exposed to extracellular matrix (ECM) components (Winkler et al., 2020), it will be important to understand in more detail the mechanisms regulating entotic cell engulfment in matrix-adherent cells.

We have recently found that the depletion of the cell adhesion receptor JAM-A in MCF7 tumor cells strongly increases cell motility and abrogates the contact inhibition of locomotion (CIL) (Kummer et al., 2022), a process that contributes to cancer cell dissemination when inappropriately regulated (Stramer and Mayor, 2016). In this study, we describe that JAM-A depletion strongly enhances entotic cell engulfment in matrix-adherent cells. Our results link deregulated motility and perturbed CIL to entotic cell engulfment, and they identify JAM-A as a central regulator of these processes.

## RESULTS

### Loss of JAM-A promotes homotypic cell engulfment

Using one-dimensional (1D) kinematic assays, in which cells are cultured on functionalized stripes of 5 μm width to promote cell collisions (Figure 1A), we have recently found that the absence of JAM-A in MCF7 cells results in increased motility as well as in a severely impaired contact inhibition of locomotion (CIL) response when cells collide with other cells (Kummer et al., 2022). The analysis of the underlying molecular mechanism revealed that JAM-A recruits c-Src regulatory kinase (Csk) to limit the activity of Src which is a key regulator of cell motility (Yeatman, 2004). During these experiments, we observed that when JAM-A-depleted cells migrated across collided cells, these were frequently engulfed resulting in cell-in-cell structures (Figure 1B). Confocal microscopic analyses confirmed that internalized cells were completely surrounded by the outer cells (Figure 1C). Quantification of cell engulfment indicated that the fraction of cell-in-cell structures strongly increased when JAM-A KD MCF7 cells collided with wildtype (WT) MCF7 cells (KD - WT collisions) as compared to collisions between control KD MCF7 cells and WT MCF7 cells (Ctrl-WT collisions) (Figure 1D). These observations suggested that the disturbed CIL response after the depletion of JAM-A facilitates homotypic cell engulfment.

### Loss of JAM-A facilitates entosis

We next aimed to characterize the cell-in-cell structures observed after JAM-A depletion in detail. We focused on entosis, a cell-in-cell phenomenon that is characterized as an invasive process and that has been found to occur at low frequencies (1.5-2%) in matrix-adherent MCF7 cells (Garanina et al., 2017) but at relatively high frequencies (20-30%) in matrix-deprived MCF7 cells (Overholtzer et al., 2007). During entosis, the invading cell ends up in a membrane-bounded compartment that is positive for Lamp1 and β-catenin (Overholtzer et al., 2007). In most cases, the internalized cells are degraded by lysosomal enzymes within the Lamp1-positive compartment; however, escape of the inner cell, as well as inner cell division, have also been observed (Krishna and Overholtzer, 2016; Overholtzer et al., 2007). We found that in the vast majority of cell-in-cell structures the internalized cell was present in a compartment positive for both Lamp1 and β-catenin (Figure 2A). The internalized cells displayed various types of behavior which were previously observed during entosis, including cell fragmentation and cell death, escape from the engulfing cell, and division of the inner cell (Figure 2B and Videos S1, S2, S3, and S4). In time-lapse movies, we also observed lobe-like structures emanating from the inner cells during the process of internalization prior to complete closure (Video S1), similar to what has recently been observed during developmental entosis in *C.elegans* (Lee et al., 2019). Ultrastructural analyses indicated a firm association between the outer and the
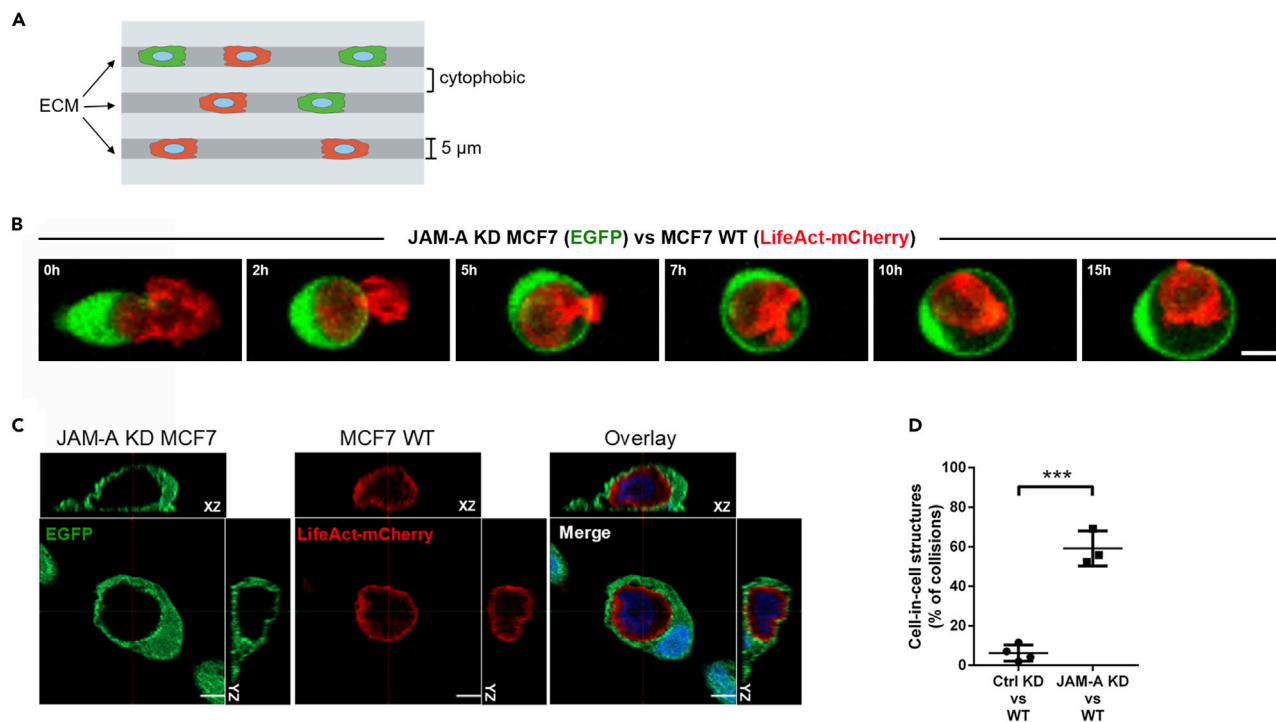
**Figure 1. Depletion of JAM-A promotes the formation of cell-in-cell structures**

(A) Cartoon of micropatterned substrates used for 1D kinematic assays. Note that cells migrate on stripes of 5 μm width coated with extracellular matrix (ECM) proteins.

(B) Engulfment of a WT MCF7 cell by a JAM-A KD MCF7 cell. Co-cultures of WT MCF7 cells (LifeAct-mCherry) and JAM-A KD MCF7 cells (EGFP) were grown on linear micropatterns of defined widths (5 μm) and observed by live microscopy for 15 h. Scale bar: 10 μm.

(C) Confocal analysis of cell engulfment. The WT MCF7 cell is completely surrounded by the JAM-A KD MCF7 cell. Scale bars: 10 μm.

(D) Quantification of cell-in-cell structures after collisions of scrambled shRNA-expressing MCF7 cells with MCF7 WT cells (Ctrl KD vs WT, n = 113, 4 independent experiments), and of collisions between JAM-A shRNA-expressing MCF7 cells with MCF7 WT cells (JAM-A KD vs WT, n = 102, 3 independent experiments). Statistical analysis was performed with unpaired Student's t-test. Data are presented as mean values ±SD ***p < 0.001.

inner cell by intercellular junctions (Figures 2C and S1), which is typically observed during entosis (Garanina et al., 2017; Overholtzer et al., 2007). The formation of cell-in-cell structures after JAM-A depletion required Rho-associated kinase (ROCK) activity (Figure 2D), which has been described to be necessary for entotic cell engulfment (Overholtzer et al., 2007). JAM-A KD – WT collisions resulted predominantly in cell-in-cell structures in which the WT cells were engulfed by the JAM-A KD cells (Figure 2E), suggesting that the increased motility of single cells combined with a loss of contact inhibition observed after JAM-A depletion (Kummer et al., 2022; Tholmann et al., 2022) prones cells to be invaded by other cells. Similar to what has been observed in the regulation of CIL (Kummer et al., 2022), we observed no difference in the rate of entosis between heterotypic JAM-A KD vs WT collisions and homotypic JAM-A KD vs JAM-A KD collisions (Figure S2), further supporting that *trans*-homhilic JAM-A interaction is required during entosis. Together, these observations suggested that the depletion of JAM-A facilitates cell engulfment of matrix-adherent cells through an entotic process, most likely as a result of loss of CIL combined with increased cell motility after JAM-A depletion.

### Regulation of entosis by JAM-A requires Tyr280 phosphorylation of JAM-A and the activity of Csk

The regulation of CIL by JAM-A requires the phosphorylation of JAM-A at Tyr280, which serves as a binding site for Csk to inhibit the activity of Src both in platelets (Naik et al., 2014) and in tumor cells (Kummer et al., 2022). To test the role of JAM-A Tyr280 phosphorylation during entosis of matrix-adherent cells, we analyzed the rate of entosis in JAM-A-depleted MCF7 cells after their reconstitution with shRNA-insensitive mouse JAM-A constructs, either mJAM-A/WT or phosphorylation-deficient mJAM-A/Y281F. Ectopic expression of mJAM-A/WT almost completely suppressed entotic cell-in-cell structures in JAM-A-depleted cells (Figure 3A). In contrast, mJAM-A/Y281F did not suppress entotic engulfment in JAM-A-depleted cells
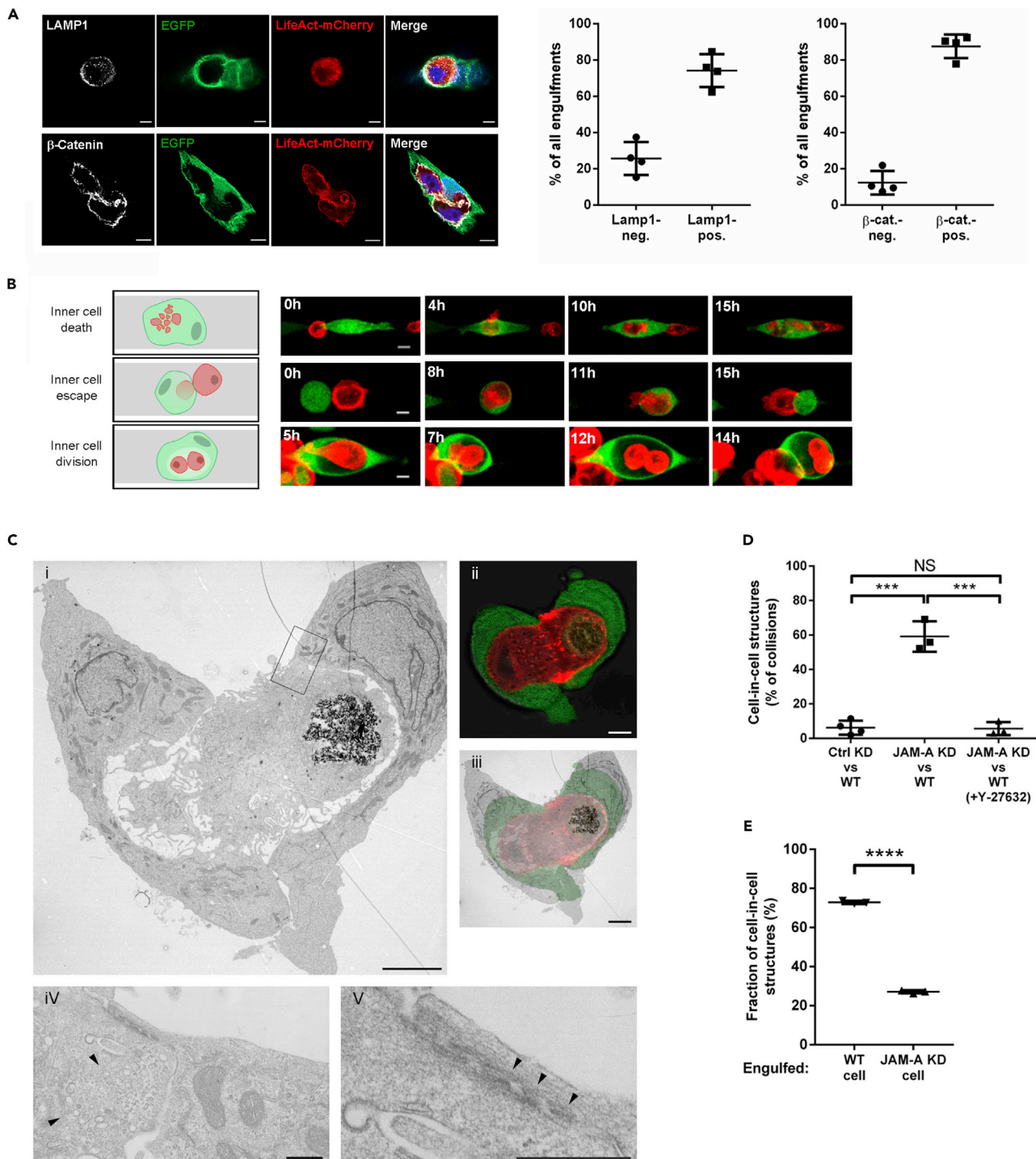
**Figure 2. Depletion of JAM-A promotes entosis**

(A) Immunofluorescence analysis of cell-in-cell structures. Co-cultures of JAM-A KD MCF7 cells (EGFP) and WT MCF7 cells (LifeAct-mCherry) were grown on linear micropatterns. After 15 h, cells were fixed and stained for Lamp1 or β-catenin. Right panels: Quantification of Lamp1- or β-catenin-positive cell-in-cell structures (n = 85 for Lamp1, n = 142 for β-catenin; 4 independent experiments). Scale bars: 10 μm.

(B) Representative images of inner cell fates after cell engulfment, which include the death of the inner cell (top), escape of the inner cell (middle), and inner cell division (bottom). Scale bars: 10 μm.

(C) Ultrastructural analysis of a cell-in-cell structure by correlative light and electron microscopy (CLEM). (i) Electron micrograph of a cell-in-cell structure after engulfment of a WT MCF7 cell (center) by two JAM-A KD MCF7 cells. (ii) Confocal section of the cell-in-cell structure shown in (i). (iii) Overlay of confocal

**Figure 2.** *Continued*

fluorescence signals (single confocal section) and electron microscopic image. Note the cellular debris inside the internalized cell reflecting the remnants of a degraded cell previously engulfed by the internalized cell. (iV) Magnification of the area delineated by the rectangle in (i). The engulfed cell shows numerous vesicles (arrowheads). (V) Magnification of the cell-cell contact area shown in (iV). Note the close apposition of the outer and inner cell membranes (arrowheads) indicative of cell-cell contacts between inner and outer cells. Scale bars: i, ii, and iii: 5 μm; iV and V: 500 nm.

(D) Quantification of cell-in-cell structures after the inhibition of ROCK (50 μM Y-27632). Co-cultures of control KD MCF7 cells and WT MCF7 cells (Ctrl KD vs WT, n = 113, 4 independent experiments), or of JAM-A KD MCF7 cells and WT MCF7 cells (JAM-A KD vs WT, n = 102, 3 independent experiments), or of JAM-A KD MCF7 cells and WT MCF7 cells in the presence of the ROCK inhibitor (JAM-A KD vs WT + Y-27632, n = 78, 3 independent experiments) were analyzed for cell-in-cell structures. Note that the data shown for control collisions (Ctrl KD vs WT) and JAM-A KD collisions (JAM-A KD vs WT) are derived from Figure 1C.

(E) Cell-in-cell structures observed after collisions between JAM-A KD MCF7 and WT MCF7 cells. JAM-A depletion results in preferential engulfment of WT MCF7 cells. Number of cell-in-cell structures analyzed: n = 59 (3 independent experiments). All statistical analyses shown in this figure were performed with unpaired Student's t-test. Data are presented as mean values ±SD. NS, not significant, ***p < 0.001, ****p < 0.0001.

(Figure 3A). As JAM-A Tyr280 phosphorylation mediates recruitment of Csk to regulate CIL in MCF7 cells (Kummer et al., 2022) and to regulate the premature activation of platelets (Naik et al., 2014), we analyzed the frequency of cell-in-cell structures after the depletion of Csk. Loss of Csk expression strongly increased the number of cell-in-cell structures (Figure 3B). In the vast majority of cell-in-cell structures, the internalized cell was present in a Lamp1- and β-catenin-positive compartment (Figures 3C and 3D), indicating that internalization occurred through entosis. In addition, similar to the observations after the depletion of JAM-A, depletion of Csk resulted in the predominant internalization of WT MCF7 cells (Figure 3E). Finally, in support of the role of Csk in entosis regulated by JAM-A, the inhibition of Src activity in JAM-A-depleted cells prevented the increase in entosis (Figure S3). Similarly, inhibiting Erk1/2, which is a downstream effector of Src and a key regulator of cell motility (Mendoza, 2013; Mendoza et al., 2011) prevented the increase in entosis in JAM-A-depleted cells (Figure S3). Together, these observations indicated that the suppression of entosis in matrix-adherent cells requires Tyr280 phosphorylation of JAM-A and the activity of Csk to suppress Src activity. As JAM-A Tyr280 phosphorylation as well as Csk activity are required to regulate CIL (Kummer et al., 2022) and to limit cell motility (Figures 3F and 3G), and as JAM-A interacts with Csk in a Tyr280-dependent manner (Kummer et al., 2022), we conclude that the loss of CIL in combination with increased cell motility facilitates entotic cell engulfment.

## JAM-A is not involved in entosis triggered by matrix deprivation

Loss of cell-matrix adhesion has been identified as a potent inducer of entosis in various tumor cell types (Buchheit et al., 2014; Ishikawa et al., 2015; Sun et al., 2014a, 2014b). As our studies in matrix-adherent cells did not exclude the possibility of a direct role of JAM-A during entosis, for example by mediating cell-cell recognition as described for E-cadherin (Sun et al., 2014a), we performed experiments in which entosis was induced by suspension culture, thereby excluding the influence of cell motility. Co-cultures of LA-GFP-labelled WT MCF7 cells and LA-mCherry-labelled JAM-A KD MCF7 cells were kept in suspension for 6 h or 12 h and analyzed for cell-in-cell structures, as described (Sun and Overholtzer, 2013) (Figure 4A). In control samples (Ctrl KD – WT co-cultures), approximately 20% of cell structures contained entotic cell-in-cell structures, both after 6 and 12 h of suspension culture (Figure 4B). The same frequency of cell-in-cell structures was observed in JAM-A KD samples (JAM-A KD – WT co-cultures) (Figure 4B). Also, we did not observe a preference for the internalization of WT cells vs JAM-A KD cells in entotic events resulting from suspension culture (Figure S4). These observations indicated that JAM-A is not involved in entosis induced by the absence of cell – matrix adhesion. They further support the notion that the increased rate of entosis after the depletion of JAM-A results from enhanced cell motility and disturbed CIL, rather than from altered cell-cell recognition.

## Loss of CIL after the depletion of JAM-A does not results in entosis in polarized epithelial cells

To test if the increased occurrence of entosis after disturbed CIL is specific to tumor cells, we performed cell collision experiments with MDCKII cells. MDCKII cells are derived from kidney distal tubules (Herzlinger et al., 1982) and are characterized by a pronounced apico-basal polarity (Dukes et al., 2011). MDCKII cells with doxycycline-regulated JAM-A shRNA expression (Tuncay et al., 2015) stably transfected with LifeAct-GFP were mixed with MDCKII WT cells stably transfected with LifeAct-mCherry and cultured on functionalized micropatterns. Collision events were classified as "opposite migration", "anergy", "contact formation", and "continuous migration" (Figure 5A), as described (Kummer et al., 2022). Depletion of JAM-A increased the number of events in which cells continued migration after collision (Figure 5B), which was very similar to what was observed in MCF7 cells (Kummer et al., 2022), indicating that JAM-A is required
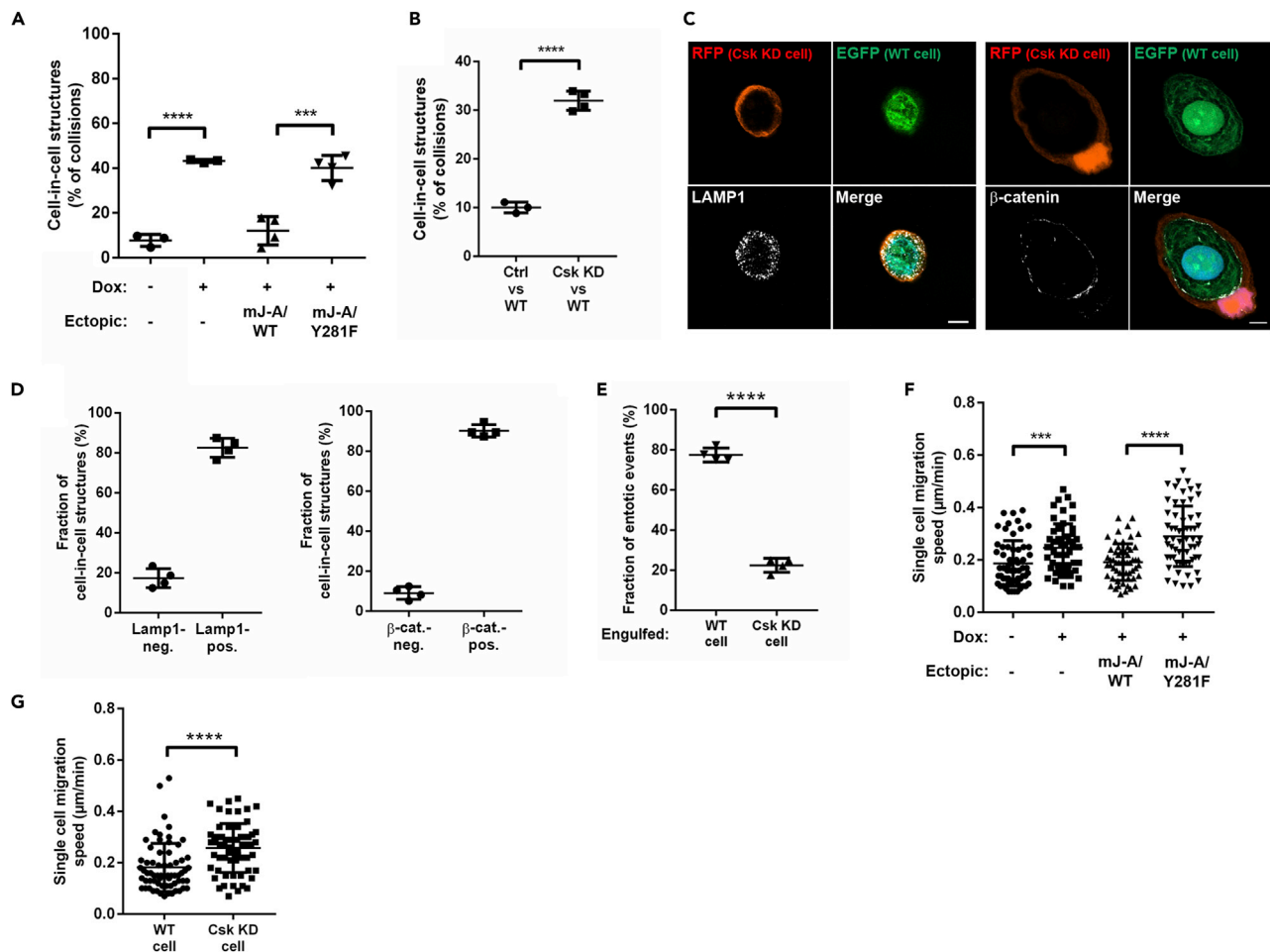
**Figure 3. Regulation of entosis requires Tyr280 phosphorylation of JAM-A and Csk activity**

(A) Quantification of cell-in-cell structures after collisions between MCF7 cells expressing JAM-A shRNAs under the regulation of a doxycycline (Dox)-regulated promoter (pEmU6-proT, - Dox, shRNA not expressed, + Dox, shRNA expressed) with MCF7 WT cells. JAM-A shRNA expressing cells were reconstituted with shRNA-resistant murine JAM-A (mJAM-A) constructs, either mJAM-A wildtype (mJ-A/WT) or Tyr281-phosphorylation-deficient mJAM-A (mJ-A/Y281F). Number of events analyzed: - Dox: 131 (3 independent experiments), + Dox: 206 (3 independent experiments), + Dox:mJAM-A/WT: 146 (4 independent experiments), + Dox:mJAM-A/Y281F: 147 (4 independent experiments).

(B) Quantification of cell-in-cell structures after collisions between control MCF7 cells (pTRIPZ-tRFP, Ctrl) or Csk KD MCF7 cells (pTRIPZ-tRFP-Csk-shRNA, Csk KD) and MCF7 WT cells (pLVTHM-EGFP, WT). Number of collisions analyzed: n = 137 cells for control experiments (Ctrl vs WT, 3 independent experiments), n = 224 for Csk KD experiments (Csk KD vs WT, 4 independent experiments).

(C) Immunofluorescence analysis for Lamp1 or β-catenin of cell-in-cell structures after collisions of Csk KD cells (RFP) and WT MCF7 cells (EGFP). Scale bars: 10 μm.

(D) Quantification of Lamp1-or β-catenin-positive cell-in-cell structures after the depletion of Csk. Number of events analyzed: n = 69 for Lamp1, n = 74 for β-catenin; 4 independent experiments.

(E) Cell-in-cell structures observed after collisions between Csk KD MCF7 and WT MCF7 cells. Csk depletion results in preferential engulfment of WT MCF7 cells. Number of collisions analyzed: n = 71 (4 independent experiments).

(F) Quantification of migration velocity of JAM-A KD cells reconstituted with mJAM-A/WT or mJAM-A/Y281F (outlined in figure part A). Note the increased migration velocity after the depletion of JAM-A, which is reversed by ectopic mJAM-A/WT but not mJAM-A/Y281F. Number of cells analyzed: - Dox: 60 (3 independent experiments), + Dox: 54 (3 independent experiments), + Dox:mJ-A/WT: 57 (4 independent experiments), + Dox:mJ-A/Y281F: 62 (4 independent experiments).

(G) Quantification of migration velocity after the depletion of Csk. Note that the depletion of Csk increases migration velocity. Number of cells analyzed: WT cells: 66 (3 independent experiments), Csk KD cells: 62 (4 independent experiments). All statistical analyses shown in this figure were performed with unpaired Student's t-test. Data are presented as mean values $\pm$ SD ***p < 0.001, ****p < 0.0001.
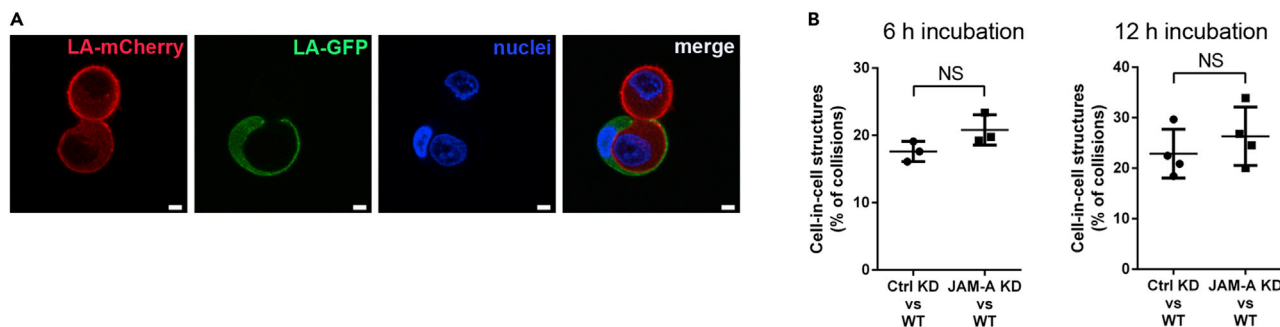
**Figure 4. JAM-A is not involved in entosis triggered by matrix deprivation**

(A) Representative immunofluorescence image of a cell-in-cell structure observed after mixed suspension culture of JAM-A KD MCF7 cells (LA-GFP) and WT MCF7 cells (LA-mCherry), Scale bar: 5 μm.

(B) Quantification of cell-in-cell structure formation in JAM-A-depleted MCF7 cells after matrix detachment. Data were obtained from mixed populations of JAM-A KD MCF7 cells (pEmU6-proT plasmid with doxycycline-regulated promoter; Ctrl KD: JAM-A shRNA expression off, JAM-A KD: JAM-A shRNA expression on; constitutive LifeAct-EGFP expression) and WT MCF7 cells (WT; constitutive LifeAct-mCherry expression) cultured for 6 h (Ctrl KD vs WT: n = 577, 3 independent experiments; JAM-A KD vs WT: n = 811, 3 independent experiments) and 12 h (Ctrl KD vs WT: n = 904, 4 independent experiments; JAM-A KD vs WT: n = 946, 4 independent experiments) in suspension as indicated. Note that JAM-A depletion has no effect on cell-in-cell structure formation. Statistical analyses shown in this figure were performed using unpaired Student's t-test. Data are presented as arithmetic means ± SD; NS, not significant.

for CIL in polarized epithelial cells. In contrast to MCF7 cells, however, the loss of CIL was not accompanied by increased entosis in these cells (Figure 5C). These observations indicated that entosis is not a general response to the loss of CIL.

## DISCUSSION

Entosis has been observed in a large variety of cancer including breast cancer (Krajcovic et al., 2011; Overholtzer et al., 2007), but is not frequently observed in matrix-adherent breast cancer cells under standard culture conditions *in vitro* (Garanina et al., 2017). Two explanations might account for this. First, we have used micropatterned substrates to perform 1D kinematic assays (Scarpa et al., 2013), in which cells migrate on stripes of 5 μm widths. Under these spatially confined culture conditions, cells cannot simply bypass other cells in response to collisions. Second, we have used MCF7 cells in which the cell adhesion receptor JAM-A has been downregulated, which results in increased cell motility and in a dysregulated CIL response in colliding cells (Kummer et al., 2022). Our observations thus provide an experimental framework to study entosis of matrix-adherent cells *in vitro*, which is expected to contribute to a better understanding of the molecular mechanisms that underly the regulation of entosis.

From our observations that JAM-A downregulation increases the rate of entosis in matrix-adherent cells but not suspension-cultured cells, we infer that JAM-A's role in the regulation of entosis is indirect and based on its regulatory function in cell motility and CIL, rather than on a function in cell-cell recognition during the entotic process. However, our recent observations on a cell-autonomous function of JAM-A suggest that JAM-A could be involved in the entotic process through additional functions independent of cell-cell adhesion. After the depletion of JAM-A, MCF7 cells display increased cell motilities associated with lower traction forces, have increased stiffness, and show increased Rac1 activities (Kummer et al., 2022). Interestingly, an increased Rac1 activity has been associated with the outer cell in entotic cell-in-cell structures, which probably serves to downregulate actomyosin contractility to facilitate the internalization of neighboring cells (Sun et al., 2014b). Through these cell-autonomous functions JAM-A could thus contribute to the entotic process. As to the mechanism of cell-cell recognition during entosis, published works indicate that entosis strongly depends on the expression of classical cadherins, such as E-cadherin or P-cadherin, and their link to the actin cytoskeleton (Sun et al., 2014a; Wang et al., 2015). Although additional cell-cell adhesion systems cannot be truled out, it seems that the cadherin-catenin complex is the primary regulator of cell-cell recognition during entosis.

Our findings thus suggest that entosis is caused by dysregulated CIL. A loss of CIL has been proposed to contribute to cancer development (Abercrombie, 1979). A loss of CIL between tumor cells and stromal cells (heterotypic CIL) facilitates cancer cell invasion into the stromal environment and thereby promotes
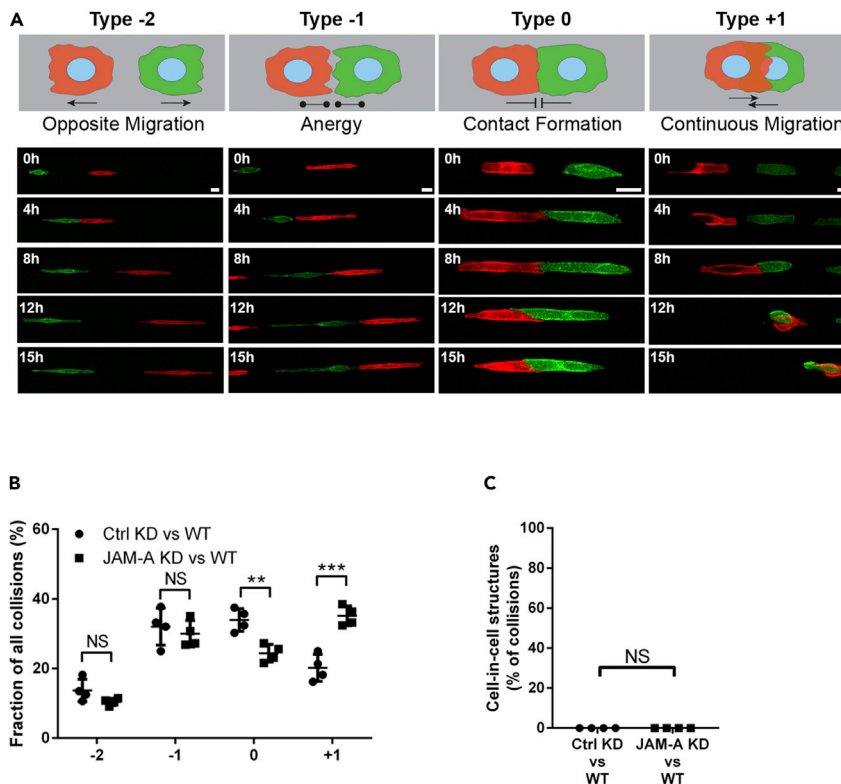
**Figure 5. Loss of JAM-A results in loss of CIL but not increased entosis in polarized epithelial cells**

(A) Classification of CIL phenotypes observed after collisions of MDCKII cells cultured on micropatterned substrates. Types of CIL responses were classified as indicated (top) and as described (Kummer et al., 2022). Scale bars: 20 μm.

(B) Quantification of CIL phenotypes after collisions of JAM-A-depleted MDCKII cells with WT MDCKII cells. Data were obtained from mixed populations of JAM-A KD MDCKII cells (pEmU6-proT plasmid with doxyxcycline-regulated promoter; Ctrl KD: JAM-A shRNA expression off, JAM-A KD: JAM-A shRNA expression on; constitutive LifeAct-EGFP expression) and WT MDCKII cells (WT; constitutive LifeAct-mCherry expression). Number of collisions analyzed: Ctrl KD vs WT: n = 106, 4 independent experiments; JAM-A KD vs WT: n = 113, 4 independent experiments).

(C) Quantification of MDCKII cell-in-cell structures after Ctrl KD vs WT collisions and after JAM-A KD vs WT collisions. Number of collisions analyzed: Ctrl KD vs WT: n = 106, 4 independent experiments; JAM-A KD vs WT: n = 113, 4 independent experiments). Note the absence of cell-in-cell structures despite disturbed CIL. All statistical analyses shown in this figure were performed with unpaired Student's t-test. Data are presented as mean values ±SD. NS, not significant, **p < 0.01, ***p < 0.001.

metastases formation (Astin et al., 2010; Paddock and Dunn, 1986). As suggested by the observations of this study, a loss of CIL between two breast cancer cells of the same type (homotypic CIL) facilitates entotic cell engulfment and thus might promote selective advantages under competitive growth conditions, which is supported by the high incidence of entosis in breast cancer (Krajcovic et al., 2011). Our findings link a dysregulation of CIL to the onset of entosis in matrix-adherent breast cancer cells.

## Limitations of the study

Our study reveals a hitherto unexplored link between loss of CIL and the occurrence of entosis. Our experiments were performed on two-dimensional linear micropatterns composed of ECM-functionalized stripes of 5-μm width that are separated by cytophobic spacers. Under these conditions repolarization and migration in other directions in response to cell-cell collision is impeded, thus favoring continuous migration and, eventually, entotic engulfment. In a three-dimensional tissue, individually migrating metastatic tumor cells may have the possibility to bypass other cells after collision, thus preventing entosis. In addition, our study involved only homotypic collisions between MCF7 tumor cells but not heterotypic collisions between MCF7 cells and other cells. In a three-dimensional tissue, individually migrating metastatic tumor cells will interact with cells of different origins. These issues should be kept in mind to avoid an overinterpretation of the findings.

## STAR★METHODS

Detailed methods are provided in the online version of this paper and include the following:

- KEY RESOURCES TABLE
- RESOURCE AVAILABILITY
  - ○ Lead contact
  - ○ Materials availability
  - ○ Data and code availability
- EXPERIMENTAL MODELS AND SUBJECT DETAILS
- METHOD DETAILS
  - ○ Cell culture and transfections
  - ○ RNA interference, plasmid vectors and constructs
  - ○ Antibodies and reagents
  - ○ Immunofluorescence microscopy
  - ○ 1D micropattern collision assays
  - ○ Cell-in-cell formation assay by suspension culture
  - ○ Correlative light – electron microscopy (CLEM)
- QUANTIFICATION AND STATISTICAL ANALYSIS

## SUPPLEMENTAL INFORMATION

Supplemental information can be found online at https://doi.org/10.1016/j.isci.2022.105144.

## AUTHOR CONTRIBUTIONS

Conception of the study: M. Schwietzer, S. Thölmann, D. Kummer, K. Ebnet. Experimentation: M. Schwietzer, S. Thölmann, A. Kaschler, L. Greune, E.-M. Thüring. Reagents: M. A. Schmidt, V. Gerke. Article: M. Schwietzer, S. Thölmann, K. Ebnet.

## DECLARATION OF INTERESTS

The authors declare no competing interests.

## REFERENCES

Abercrombie, M. (1979). Contact inhibition and malignancy. Nature 281, 259–262.

Astin, J.W., Batson, J., Kadir, S., Charlet, J., Persad, R.A., Gillatt, D., Oxley, J.D., and Nobes, C.D. (2010). Competition amongst Eph receptors regulates contact inhibition of locomotion and invasiveness in prostate cancer cells. Nat. Cell Biol. 12, 1194–1204. https://doi.org/10.1038/ncb2122.

Bozkurt, E., Düssmann, H., Salvucci, M., Cavanagh, B.L., Van Schaeybroeck, S., Longley, D.B., Martin, S.J., and Prehn, J.H.M. (2021). TRAIL

signaling promotes entosis in colorectal cancer. J. Cell Biol. 220, e202010030. https://doi.org/10.1083/jcb.202010030.

Brown, G.C., and Neher, J.J. (2012). Eaten alive! Cell death by primary phagocytosis: 'phagoptosis'. Trends Biochem. Sci. 37, 325–332. https://doi.org/10.1016/j.tibs.2012.05.002.

Buchheit, C.L., Weigel, K.J., and Schafer, Z.T. (2014). Cancer cell survival during detachment from the ECM: multiple barriers to tumour progression. Nat. Rev. Cancer 14, 632–641. https://doi.org/10.1038/nrc3789.

Dukes, J.D., Whitley, P., and Chalmers, A.D. (2011). The MDCK variety pack: choosing the right strain. BMC Cell Biol. 12, 43. https://doi.org/10.1186/1471-2121-12-43.

Durgan, J., and Florey, O. (2018). Cancer cell cannibalism: multiple triggers emerge for entosis. Biochim. Biophys. Acta Mol. Cell Res. 1865, 831–841. https://doi.org/10.1016/j.bbamcr.2018.03.004.

Fais, S., and Overholtzer, M. (2018). Cell-in-cell phenomena in cancer. Nat. Rev. Cancer 18,

758–766. https://doi.org/10.1038/s41568-018-0073-9.

Finicle, B.T., Jayashankar, V., and Edinger, A.L. (2018). Nutrient scavenging in cancer. Nat. Rev. Cancer *18*, 619–633. https://doi.org/10.1038/s41568-018-0048-x.

Florey, O., Kim, S.E., Sandoval, C.P., Haynes, C.M., and Overholtzer, M. (2011). Autophagy machinery mediates macroendocytic processing and entotic cell death by targeting single membranes. Nat. Cell Biol. *13*, 1335–1343. https://doi.org/10.1038/ncb2363.

Frisch, S.M., and Francis, H. (1994). Disruption of epithelial cell-matrix interactions induces apoptosis. J. Cell Biol. *124*, 619–626. https://doi.org/10.1083/jcb.124.4.619.

Garanina, A.S., Kisurina-Evgenieva, O.P., Erokhina, M.V., Smirnova, E.A., Factor, V.M., and Onishchenko, G.E. (2017). Consecutive entosis stages in human substrate-dependent cultured cells. Sci. Rep. *7*, 12555. https://doi.org/10.1038/s41598-017-12867-6.

Hamann, J.C., Surcel, A., Chen, R., Teragawa, C., Albeck, J.G., Robinson, D.N., and Overholtzer, M. (2017). Entosis is induced by glucose starvation. Cell Rep. *20*, 201–210. https://doi.org/10.1016/j.celrep.2017.06.037.

Herzlinger, D.A., Easton, T.G., and Ojakian, G.K. (1982). The MDCK epithelial cell line expresses a cell surface antigen of the kidney distal tubule. J. Cell Biol. *93*, 269–277. https://doi.org/10.1083/jcb.93.2.269.

Ishikawa, F., Ushida, K., Mori, K., and Shibanuma, M. (2015). Loss of anchorage primarily induces non-apoptotic cell death in a human mammary epithelial cell line under atypical focal adhesion kinase signaling. Cell Death Dis. *6*, e1619. https://doi.org/10.1038/cddis.2014.583.

Krajcovic, M., Johnson, N.B., Sun, Q., Normand, G., Hoover, N., Yao, E., Richardson, A.L., King, R.W., Cibas, E.S., Schnitt, S.J., et al. (2011). A non-genetic route to aneuploidy in human cancers. Nat. Cell Biol. *13*, 324–330. https://doi.org/10.1038/ncb2174.

Krishna, S., and Overholtzer, M. (2016). Mechanisms and consequences of entosis. Cell. Mol. Life Sci. *73*, 2379–2386. https://doi.org/10.1007/s00018-016-2207-0.

Kummer, D., Steinbacher, T., Thölmann, S., Schwietzer, M.F., Hartmann, C., Horenkamp, S., Demuth, S., Peddibhotla, S.S.D., Brinkmann, F., Kemper, B., et al. (2022). A JAM-A-tetraspanin-alphavbeta5 integrin complex regulates contact inhibition of locomotion. J. Cell Biol. *221*, e202105147. https://doi.org/10.1083/jcb.202105147.

Lee, Y., Hamann, J.C., Pellegrino, M., Durgan, J., Domart, M.C., Collinson, L.M., Haynes, C.M., Florey, O., and Overholtzer, M. (2019). Entosis controls a developmental cell clearance in C. elegans. Cell Rep. *26*, 3212–3220.e4. https://doi.org/10.1016/j.celrep.2019.02.073.

Lugini, L., Lozupone, F., Matarrese, P., Funaro, C., Luciani, F., Malorni, W., Rivoltini, L., Castelli, C., Tinari, A., Piris, A., et al. (2003). Potent phagocytic activity discriminates metastatic and primary human malignant melanomas: a key role of ezrin. Lab. Invest. *83*, 1555–1567.

Mackay, H.L., Moore, D., Hall, C., Birkbak, N.J., Jamal-Hanjani, M., Karim, S.A., Phatak, V.M., Piñon, L., Morton, J.P., Swanton, C., et al. (2018). Genomic instability in mutant p53 cancer cells upon entotic engulfment. Nat. Commun. *9*, 3070. https://doi.org/10.1038/s41467-018-05368-1.

Mendoza, M.C. (2013). Phosphoregulation of the WAVE regulatory complex and signal integration. Semin. Cell Dev. Biol. *24*, 272–279. https://doi.org/10.1016/j.semcdb.2013.01.007.

Mendoza, M.C., Er, E.E., Zhang, W., Ballif, B.A., Elliott, H.L., Danuser, G., and Blenis, J. (2011). ERK-MAPK drives lamellipodia protrusion by activating the WAVE2 regulatory complex. Mol. Cell *41*, 661–671. https://doi.org/10.1016/j.molcel.2011.02.031.

Merino, M.M., Levayer, R., and Moreno, E. (2016). Survival of the fittest: essential roles of cell competition in development, aging, and cancer. Trends Cell Biol. *26*, 776–788. https://doi.org/10.1016/j.tcb.2016.05.009.

Naik, M.U., Caplan, J.L., and Naik, U.P. (2014). Junctional adhesion molecule-A suppresses platelet integrin alphaIIbbeta3 signaling by recruiting Csk to the integrin-c-Src complex. Blood *123*, 1393–1402. https://doi.org/10.1182/blood-2013-04-496232.

Overholtzer, M., Mailleux, A.A., Mouneimne, G., Normand, G., Schnitt, S.J., King, R.W., Cibas, E.S., and Brugge, J.S. (2007). A nonapoptotic cell death process, entosis, that occurs by cell-in-cell invasion. Cell *131*, 966–979. https://doi.org/10.1016/j.cell.2007.10.040.

Paddock, S.W., and Dunn, G.A. (1986). Analysing collisions between fibroblasts and fibrosarcoma cells: fibrosarcoma cells show an active invasionary response. J. Cell Sci. *81*, 163–187.

Scarpa, E., Roycroft, A., Theveneau, E., Terriac, E., Piel, M., and Mayor, R. (2013). A novel method to study contact inhibition of locomotion using micropatterned substrates. Biol. Open *2*, 901–906. https://doi.org/10.1242/bio.20135504.

Stramer, B., and Mayor, R. (2016). Mechanisms and in vivo functions of contact inhibition of locomotion. Nat. Rev. Mol. Cell Biol. *18*, 43–55. https://doi.org/10.1038/nrm.2016.118.

Sun, Q., Cibas, E.S., Huang, H., Hodgson, L., and Overholtzer, M. (2014a). Induction of entosis by epithelial cadherin expression. Cell Res. *24*, 1288–1298. https://doi.org/10.1038/cr.2014.137.

Sun, Q., Luo, T., Ren, Y., Florey, O., Shirasawa, S., Sasazuki, T., Robinson, D.N., and Overholtzer, M. (2014b). Competition between human cells by entosis. Cell Res. *24*, 1299–1310. https://doi.org/10.1038/cr.2014.138.

Sun, Q., and Overholtzer, M. (2013). Methods for the study of entosis. Methods Mol. Biol. *1004*, 59–66. https://doi.org/10.1007/978-1-62703-383-1_5.

Tholmann, S., Seebach, J., Otani, T., Florin, L., Schnittler, H., Gerke, V., Furuse, M., and Ebnet, K. (2022). JAM-A interacts with alpha3beta1 integrin and tetraspanins CD151 and CD9 to regulate collective cell migration of polarized epithelial cells. Cell. Mol. Life Sci. *79*, 88. https://doi.org/10.1007/s00018-022-04140-5.

Tuncay, H., Brinkmann, B.F., Steinbacher, T., Schürmann, A., Gerke, V., Iden, S., and Ebnet, K. (2015). JAM-A regulates cortical dynein localization through Cdc42 to control planar spindle orientation during mitosis. Nat. Commun. *6*, 8128. https://doi.org/10.1038/ncomms9128.

Wang, M., Ning, X., Chen, A., Huang, H., Ni, C., Zhou, C., Yu, K., Lan, S., Wang, Q., Li, S., et al. (2015). Impaired formation of homotypic cell-in-cell structures in human tumor cells lacking alpha-catenin expression. Sci. Rep. *5*, 12223. https://doi.org/10.1038/srep12223.

Wang, S., He, M., Li, L., Liang, Z., Zou, Z., and Tao, A. (2016). Cell-in-cell death is not restricted by caspase-3 deficiency in MCF-7 cells. J. Breast Cancer *19*, 231–241. https://doi.org/10.4048/jbc.2016.19.3.231.

Winkler, J., Abisoye-Ogunniyan, A., Metcalf, K.J., and Werb, Z. (2020). Concepts of extracellular matrix remodelling in tumour progression and metastasis. Nat. Commun. *11*, 5120. https://doi.org/10.1038/s41467-020-18794-x.

Yeatman, T.J. (2004). A renaissance for SRC. Nat. Rev. Cancer *4*, 470–480.

## STAR★METHODS

### KEY RESOURCES TABLE

| REAGENT or RESOURCE | SOURCE | IDENTIFIER |
|---|---|---|
| **Antibodies** | | |
| anti LAMP1 | Developmental Studies Hybridoma Bank | #H4A3; RRID: AB_2296838 |
| anti β-Catenin | BD Biosciences | #610154; RRID: AB_397555 |
| Donkey anti-Mouse IgG (H+L) Highly Cross-Adsorbed Secondary Antibody, Alexa Fluor™ Plus 488 | Invitrogen | #A-32766 |
| Goat anti-Mouse IgG (H+L) Highly Cross-Adsorbed Secondary Antibody, Alexa Fluor™ 594 | Invitrogen | #A-11032 |
| Goat anti-Mouse IgG (H+L) Highly Cross-Adsorbed Secondary Antibody, Alexa Fluor™ 647 | Invitrogen | #A-21236 |
| **Bacterial and virus strains** | | |
| NEB5α | NEB | #C2987H |
| Stbl3 | Dr. Hans Schnittler, University Hospital Münster, Germany | NA |
| **Chemicals, peptides, and recombinant proteins** | | |
| Recombinant human vitronectin | Peprotech | #140-09 |
| Fibronectin isolated from human plasma | Sigma-Aldrich | #F2006 |
| Rat tail type I collagen | Advanced BioMatrix | #5153 |
| Methylcellulose | Sigma-Aldrich | #M7027 |
| PolyHEMA | Sigma-Aldrich | #P3932 |
| PP2 | Sigma-Aldrich | #529573 |
| CI-1040 | Atriva Therapeutics GmbH | personal gift of Dr. André Schreiber, IMV, Münster |
| RPMI | Thermo Fisher | #32404014 |
| DMEM | Pan Biotech | #P04-03500 |
| FBS | Capricorn Scientific | FBS-11A |
| PBS | PAN Biotech | P04-36500 |
| L-Glutamine | Lonza AG | BE17-605E |
| Penicillin/Streptomycin | Lonza AG | DE17-602E |
| Na-pyruvate | Sigma-Aldrich | S8636-100ML |
| non-essential amino acids | Capricorn Scientific | NEAA-B |
| 2,4,diamidino-2-phenylindole (DAPI) | Sigma-Aldrich | #D9542 |
| Paraformaldehyde | Sigma-Aldrich | #P6148 |
| Triton X-100 | Applichem | A1388,1000 |
| Tween-20 | Applichem | A1389,1000 |
| BSA | Roth | 8076.3 |
| Blasticidin | InvivoGen | ant-bl-1 |
| G418 | AppliChem | A6798,0050 |
| Puromycin-dihydrochloride | AppliChem | A2856,0100 |
| Glycine | Applichem | A1067,5000 |
| Mowiol 4-88 | Sigma-Aldrich | #81381 |
| Glutaraldehyde, 25% (EM grade) | Polysciences | #01909-10 |

*(Continued on next page)*

*Continued*

| REAGENT or RESOURCE | SOURCE | IDENTIFIER |
|---|---|---|
| Osmium tetroxide, crystalline 99.95% | Polysciences | #0223A-5 |
| Uranyl Acetate 98% | Polysciences | # 21447-25 |
| Epon | Agar Scientific | #AGR1031 |
| Pb(II) citrate | Sigma-Aldrich | #15326 |
| D-PBS | Sigma-Aldrich | #D5652 |
| **Critical commercial assays** | | |
| CYTOOchips™ Motility Ax18 | CYTOO INC, Grenoble, France | #10-031-00-18 |
| Ibidi μ-Slide 2 well glass bottom | Ibidi | #80287 |
| ditabis imaging plate system | ditabis Pforzheim, Germany | NA |
| **Experimental models: Cell lines** | | |
| MCF7: human adenocarcioma cells derived from a female patient | ATCC | #HTB-22 RRID: CVCL_0031 |
| HEK293T: human epithelial-like cells derived from a femal embryonic kidney | ATCC | #CRL-3216 RRID: CVCL_0063 |
| MDCKII: canine epithelial cells derived from the kidney (distal tubule) of a female cocker spaniel | Sigma-Aldrich | #00062107 RRID: CVCL_0424 |
| **Oligonucleotides** | | |
| 5'-GAAGTGAAGGAGAATTCAA-3', hJAM-A shRNA | in pLVTHM | NA |
| 5'-CCAGTAAGAAGGTGATTTA-3', cJAM-A shRNA | in pEmU6-proT | NA |
| 5'-GAAGTGAAGGAGAATTCAA-3', hJAM-A shRNA | in pEmU6-proT | NA |
| 5'-TAATGAGGCGCGTACAGAG-3', hCsk shRNA | in pTRIPZ (Horizon-Dharmacon) | #RHS4696-200701764 |
| 5'-CCTAAGGTTAAGTCGCCCTCG-3', scrambled shRNA | in pLKO.1 (Addgene) | #1864 |
| **Recombinant DNA** | | |
| pLVTHM | Addgene | #12247 |
| psPAX2 | Addgene | #12260 |
| pMD2.G | Addgene | #12259 |
| pEmU6-proT | Dr. Karl Matter, University College London, UK | NA |
| pTRIPZ | Horizon-Dharmacon | #RHS4696-200701764 |
| pLKO.1 | Addgene | #10878 |
| pFUGW_LifeAct-eGFP | Dr. Hans Schnittler, University Hospital Münster, Germany | NA |
| pLV-PGK-Puro_ LifeAct-mCherry | Dr. Henner Farin Institute for Tumor Biology and Experimental Therapy | NA |
| pCDH-CMV-MCS-EF1-Puro | SBI, Mountain View, CA | #CD510B-1-SB |
| **Software and algorithms** | | |
| GraphPad Prism 5.0 | GraphPaD Software | http://www.ddooo.com/softdown/44298.htm |
| Image J | ImageJ Software | https://imagej/nih/gov/ij/ |
| Imaris | Bitplane, Version 9.1.2 | http://www.bitplane.com/ |

## RESOURCE AVAILABILITY

### Lead contact

Furher information and requests for resources and reagents should be directed to and will be fulfilled by the lead contact, Klaus Ebnet (ebnetk@uni-muenster.de).

### Materials availability

This study did not generate new unique reagents.

### Data and code availability

- All data produced or analyzed in this study (including movies) are included in the published article or in the supplemental information files.

- This study did not generate new codes.

- Original western blot images and microscopy data reported in this paper will be shared by the lead contact upon request. Any additional information required to reanalyze the data reported in this paper is available from the lead contact upon reasonable request.

## EXPERIMENTAL MODELS AND SUBJECT DETAILS

MCF7 cells (ATCC #HTB-22) are human adenocarcioma cells derived from a female patient. Cells were grown in at 37°C in a humidified atmosphere in RPMI 1640 medium without phenol red (Thermo Fisher #32404014) containing 10% FCS, 2 mM glutamine, 100 U/ml penicillin and 100 U/ml streptomycin, 1 mM Na-pyruvate and 1:100 non-essential amino acids (Capricorn Scientific). The generation of MCF7 cell lines expressing JAM-A shRNAs, Csk shRNAs, and fluorescent proteins (EGFP, LifeAct-mCherry, LifeAct-GFP) have been described in detail before (Kummer et al., 2022). MCF7 WT cells were used as collision partners in 1D micropattern collision assays and in suspension assyas; MCF7 cells with constitutive (pLVTHM) or inducible JAM-A KD (pEmU6proT, + Dox, shRNA expression On, - Dox, shRNA expression off) were used as collision partners in 1D micropattern collision assays and in suspension assays. HEK293T (ATCC #CRL-3216) cells are human epithelial-like cells derived from embryonic kidney. Cells were grown in DMEM (PAN Biotech #P04-03500) containing 10% FCS, 2 mM glutamine, 100 U/ml penicillin and 100 U/ml streptomycin. Cells were used for the generation of pseudovirus particles. MDCKII cells are canine epithelial cells derived from the collecting duct of a female cocker spaniel (Herzlinger et al., 1982). MDCKII wildtype cells (Sigma-Aldrich, Munich, Germany, Sigma cat. #00062107) were grown in DMEM containing 10% FCS, 1% glutamine, 100 U/ml penicillin, 100 μg/mL streptomycin. MDCKII wildtype cells were stably transfected with LifeAct-mCherry and used as collision partners in 1D micropattern collision assays. Cells were grown in DMEM containing 10% FCS, 1% glutamine, 100 U/ml penicillin, 100 μg/mL streptomycin. The generation of MDCKII cell lines expressing canine-specific JAM-A shRNAs under a doxycycline-regulated promoter have been described in detail before (Tuncay et al., 2015). Cells were stably transfected with LifeAct-GFP. Stably LifeAct-GFP-transfected MDCKII cells with inducible JAM-A shRNA expression were used in collision assays as JAM-A KD cells (+ doxycycline) or control KD cells (- doxycycline). All cell lines used in this study were routinely tested and found to be negative for mycoplasm contamination.

## METHOD DETAILS

### Cell culture and transfections

Transient transfections of siRNAs were performed using Lipofectamine RNAiMAX (Thermo Fisher Scientific) according to the manufacturer's instructions. Lentiviral particles for the generation of stably transfected cell lines expressing either shRNAs or cDNAs were generated by cotransfection of HEK293T cells with the lentiviral vector and the packaging vectors psPAX2 and pMD2.G (kindly provided by Dr. Didier Trono, Addgene plasmids #12260 and #12259) in a ratio of 3:2:1 into HEK293T cells. Lentiviral particles-containing HEK293T supernatants were harvested one day after transfection. MCF7 and MDCKII target cells were incubated with lentiviral supernatants for 24 h. Transduced cells were maintained in standard culture medium supplemented with 1 μg/mL puromycin (AppliChem). MCF7 cells and MDCKII cells expressing JAM-A shRNAs under a doxycycline-regulated promoter were generated by electroporation of cells with plasmid pEmU6-proT (provided by Dr. Karl Matter). Transfectants were selected with 500 ug/ml G418 (AppliChem) and 7 ug/ml blasticidin (InvivoGen).

### RNA interference, plasmid vectors and constructs

The following siRNAs and shRNAs were used: hJAM-A shRNA 5'-GAAGTGAAGGAGAATTCAA-3' (in pLVTHM (Addgene #12247), canine shRNA 5'-CCAGTAAGAAGGTGATTTA-3' in pEmU6-proT; hCSK shRNA 5'-TAATGAGGCGCGTACAGAG-3' in pTRIPZ (Dharmacon RHS4696-200701764); scrambled shRNA 5'-CCTAAGGTTAAGTCGCCCTCG-3' in pLKO.1 (Addgene #1864). The following constructs were used: LifeAct-eGFP in pFUGW (provided by Dr. H. Schnittler), LifeAct-mCherry in pLV-PGK-Puro (provided by Dr. H. Farin); Flag-mJAM-A/WT, Flag-mJAM-A/Y281F in pCDH-CMV-MCS-EF1-Puro (SBI, Mountain

View, CA). The efficiencies and specificities of the JAM-A and Csk shRNAs as well as the expression levels of ectopically expressed mJAM-A constructs (mJAM-A/WT, mJAM-A/Y281F) are depicted in Figure S5.

### Antibodies and reagents

The following antibodies were used in this study: mouse mAb anti β-catenin (BD TL 610154, Lot #9315374, IF 1:600), mouse mAb anti LAMP1 clone H4A3 (Developmental Studies Hybridoma Bank, IF 1:600). Reagents: recombinant human vitronectin (VN, Peprotech 140-09), fibronectin (FN, isolated from human plasma, SA #F2006), rat tail type I collagen (Advanced BioMatrix #5153), methylcellulose (Sigma-Aldrich #M7027), poly(2-hydroxyethyl methacrylate (polyHEMA, Sigma-Aldrich #P3932); Src inhibitor PP2 (Sigma-Aldrich #529573); MEK1/2 inhibitor CI-1040 (Atriva Therapeutics GmbH, Tübingen, Germany, kindly provided by Dr. A. Schreiber, Institute of Molecular Virology, ZMBE, Münster).

### Immunofluorescence microscopy

For immunofluorescence microscopy, cells were grown on VN-coated (MCF7) or collagen-coated (HEK293T) glass slides. Cells were washed with PBS and fixed with 4% paraformaldehyde (PFA, Sigma-Aldrich) for 7 min. For permeabilization, PFA-fixed cells were incubated with PBS containing 0.5% Triton X-100 for 15 min. Cells were washed with 100 mM glycine in PBS, blocked for 1 h in blocking buffer (PBS, 10% FCS, 0.2% Triton X-100, 0.05% Tween-20, 0.02% BSA) and then incubated with primary antibodies in blocking buffer for 1 h at room temperature (RT) or overnight at 4°C. After incubation, cells were washed three times with PBS and incubated with fluorochrome (AlexaFluor488, AlexaFluor594 and AlexaFluor647)-conjugated, highly cross-adsorbed secondary antibodies (Invitrogen) for 2 h at RT. DNA was stained with 2,4,diamidino-2-phenylindole (DAPI, Sigma-Aldrich). Samples were washed with PBS and mounted in fluorescence mounting medium (Mowiol 4–88, Sigma-Aldrich). Immunofluorescence microscopy was performed using the confocal microscopes LSM780 and LSM800 Airyscan (both from Carl Zeiss, Jena, Germany) equipped with the objectives Plan-Apochromat ×40/1.3 oil differential interference contrast and Plan-Apochromat x 63/1.4 oil differential interference contrast (Carl Zeiss). Image processing and quantification was performed using ImageJ and Imaris (Bitplane, Version 9.1.2) software.

### 1D micropattern collision assays

For one-dimensional (1D) collision assays (Scarpa et al., 2013), chips with micropatterns of linear tracks of 5 μm width (CYTOOchips™ Motility Ax18, CYTOO INC, Grenoble, France) were used. Co-cultures of knockdown cells (JAM-A KD MCF7, Csk KD MCF7, JAM-A KD MDCKII) or the respective control cells mixed at a 1:1 ratio with wildtype cells (WT MCF7, WT MDCKII) were seeded on functionalized (VN, FN) micropatterned stripes at $5 \times 10^4$ cells/ml. Cells were allowed to adhere to the surface for 2 h, then observed by live cell microscopy over a period of 15 h with image acquisition at 10-min intervals. Live cell microscopy was performed using the LSM780 (Carl Zeiss) confocal microscope equipped with a Plan-Neofluar × 20/0.5 objective. In some cases, cells were fixed after live cell image acquisition, stained with antibodies and analyzed by confocal microscopy (0.36 μm sections) using a 63x Plan-Apochromat oil-immersion objective (LSM800 Airyscan). Migration velocity of individual cells were analyzed semi-automatically using the TrackMate Plugin for ImageJ. For the analysis of CIL, cell behavior after collision was categorized as follows: Type -2 (opposite migration), type -1 (anergy, i.e. stop of migration without cell-cell contact formation), type 0 (cell-cell contact formation), type +1 (continuous migration, i.e. migration across collided cell). Statistical analyses were performed with data from at least three independent experiments using unpaired, two-tailed Student's $t$-tests, data are expressed as arithmetic means $\pm$ SD.

### Cell-in-cell formation assay by suspension culture

For cell-in-cell formation assays after matrix detachment, MCF7 cells transfected with either LifeAct-EGFP (MCF7 cells with doxycycline-regulated expression of JAM-A shRNAs, pEmU6-proT) or LifeAct-mCherry (MCF7 WT) were trypsinized to a single cell suspension and mixed at a 1:1 ratio at 50.000 cells/ml in growth media supplemented with 0.5% methylcellulose. The cell mixture was cultured in suspension for 6 h or 12 h on tissue culture dishes coated with polyHEMA. Afterwards, the cell suspension was transferred to poly-HEMA-coated microscope slides (Ibidi μ-Slide 2 well glass bottom, Ibidi #80287) for live-cell-microscopy. Cell-in-cell structures were analyzed by confocal live-cell microscopy (LSM780, Carl Zeiss) on the basis of LifeAct-EGFP and LifeAct-mCherry fluorescence signals. Cellular aggregates which occurred especially after 12 h of suspension culture were excluded from the analysis. For quantification of cell-in-cell structures, between 136 and 347 cells from randomly chosen fields for each condition per experiment were analyzed.

Statistical analyses were performed with data from three to four independent experiments using unpaired, two-tailed Student's $t$-tests, data are expressed as arithmetic means $\pm$ SD.

### Correlative light – electron microscopy (CLEM)

EGFP-positive JAM-A KD MCF7 cells and LifeAct-mCherry-expressing MCF7 WT cells were mixed and grown on glass cover slides. Cell-in-cell structures were identified by confocal microscopy prior to fixation. Samples were subsequently fixed in 2.5% glutaraldehyde (Polysciences Europe GmbH, Hirschberg, Germany) in D-PBS (Sigma-Aldrich), post-fixed in 1% osmium tetroxide (Polysciences), block-stained with 0,5% uranyl acetate (Polysciences), dehydrated and flat-embedded in Epon 812 (Agar Scientific, Stansted, UK). Areas of interest were selected based on the fluorescence images and embedded in gelatine capsules (Polysciences). After polymerization, 60-nm ultrathin sections were counterstained with uranyl acetate (Polysciences) and lead (Pb(II) citrate, Sigma-Aldrich). Samples were analyzed at 80 kV on a FEI-Tecnai 12 electron microscope (FEI, Eindhoven, Netherlands). Images of selected areas were documented with ditabis imaging plates (Ditabis, Pforzheim, Germany).

### QUANTIFICATION AND STATISTICAL ANALYSIS

Results are expressed as arithmetic means $\pm$ SD as indicated. To test the normality of data sample distributions, the D'Agostino-Pearson normality test was used. Data were statistically compared using unpaired, two-tailed Student's $t$ test. Statistical analyses were performed using GraphPad Prism version 6 (GraphPad Software, San Diego, CA). p-values are indicated as follows: $*p < 0.05$, $**p < 0.01$, $***p < 0.001$ and $****p < 0.0001$.